



OPEN Unique formation of organic glass from a human brain in the Vesuvius eruption of 79 CE

Guido Giordano¹✉, Alessandra Pensa^{1,2}, Alessandro Vona¹, Danilo Di Genova^{3,4}, Raschid Al-Mukadam³, Claudia Romano¹, Joachim Deubener³, Alessandro Frontoni¹ & PierPaolo Petrone⁵

Glass forms when a liquid is fast cooled preventing crystallization, across a reversible process known as the glass transition. Organic tissues are commonly preserved as glass by processes of vitrification at very low temperatures, known as cryopreservation, and can return to their original soft state when heated back to ambient temperature. It would therefore be impossible to find organic glass embedded in volcanic deposits that have reached several hundred of Celsius degrees. Here we demonstrate that material with glassy appearance found within the skull of a seemingly male human body entombed within the hot pyroclastic flow deposits of the 79 CE Vesuvius eruption formed by a unique process of vitrification of his brain at very high temperature, and is the only such occurrence on Earth. Calorimetric analyses show that the temperature at which the brain transformed into glass was well above 510 °C, implying that the body was exposed to the passage and vanishing of a short-lived, dilute and much hotter pyroclastic flow, explaining its early fast heating and the following very fast cooling. The glass that formed as a result of such a unique process attained a perfect state of preservation of the brain and its microstructures.

Main

Natural glasses are uncommon but not rare on Earth^{1–9}. The glass state represents a non-equilibrium, non-crystalline condensed phase of matter characterized by the presence of a glass transition¹. Glass formation occurs as the cooling path of a liquid leads to an increase in its structural relaxation time, thereby circumventing the crystallization process and entering the phase referred to as the glass transition interval, during which the liquid properties deviate from equilibrium. The temperature at which this deviation occurs is known as fictive temperature T_f ². T_f is not a fixed temperature, as it depends, for a given liquid, on the cooling rate, i.e., the faster the cooling rate, the higher T_f ^{2–4,10–14}. Glasses can unlock their thermal history if heated above T_f . Given such conditions of formation, natural glasses can only occur on Earth if their T_f is above ambient temperature. This is the case of silicic glasses that commonly form in volcanic environments from the fast cooling of viscous magma (eruptive temperatures 700–1200 °C depending on chemical composition) in subaerial or subaqueous conditions (e.g., obsidian)^{15–17}. More rarely silicic glasses may form by the melting of rocks across slipping faults or at the high-shear base of landslides and then their quenching as pseudotachylites¹⁸ or may also form when lightning strikes locally melt rocks which then quench as fulgurites¹⁹. In all these cases the silicate liquid temperatures are several hundred to above one thousand degrees Celsius, and the relative T_f is in the same range.

By contrast, organic tissues are largely made of water, that is a liquid at ambient temperature, so that they can only be vitrified by quenching and storage well below 0 °C⁶. In cryopreservation, vitrification refers to the rapid cooling of organs to a stable, ice-free, glass-like state²⁰ by immersion in liquid nitrogen to be fully preserved and returnable to its original state⁵; in this condition, the system becomes a glass, acquiring the properties of a solid but retaining the molecular structure of soft tissues typically at T_f of -120 °C (± 10 °C)^{5,21}. Consequently, no glasses obtained from the quenching of biological soft tissues can exist at ambient temperature as they would

¹Dipartimento di Scienze, Università Roma Tre, Largo San Leonardo Murialdo 1, Roma 00146, Italy. ²Istituto Superiore per la Protezione e la Ricerca Ambientale, Via Vitaliano Brancati 48, Roma 00144, Italy. ³Technische Universität Clausthal, Adolph-Roemer-Straße 2A, 38678 Clausthal-Zellerfeld, Germany. ⁴CNR-ISSMC Istituto di Scienza, Tecnologia e Sostenibilità per lo sviluppo dei Materiali Ceramici, Via Granarolo, 64, 48018 Faenza, RA, Italy. ⁵Dipartimento di Scienze Biomediche Avanzate, Università di Napoli Federico II, Naples, Italy. ✉email: guido.giordano@uniroma3.it

cross back above their T_g and return to soft materials, which is why no such occurrences exist as natural glasses on Earth.

However, there is one exception. Unique apparently vitrified remnants of organic material, recognized as a human brain in origin, have been recently identified in the skull of a victim from the ancient Roman city of Herculaneum⁷, buried by the pyroclastic flow deposits that also destroyed Pompeii in 79 CE, during the most famous Plinian eruption of Vesuvius^{22–26}. This unique finding belongs to a victim of the eruption found lying in his bed (Fig. 1a) inside the Collegium Augustalium (lat. 40°48'24"N, long. 14°20'52"E). He was a young male of about 20 years-old, believed to have been the guardian of the Collegium, a public building dedicated to the worship of Emperor Augustus, located on the city's main street (Decumanus maximus) (Fig. 1b)²⁷. The

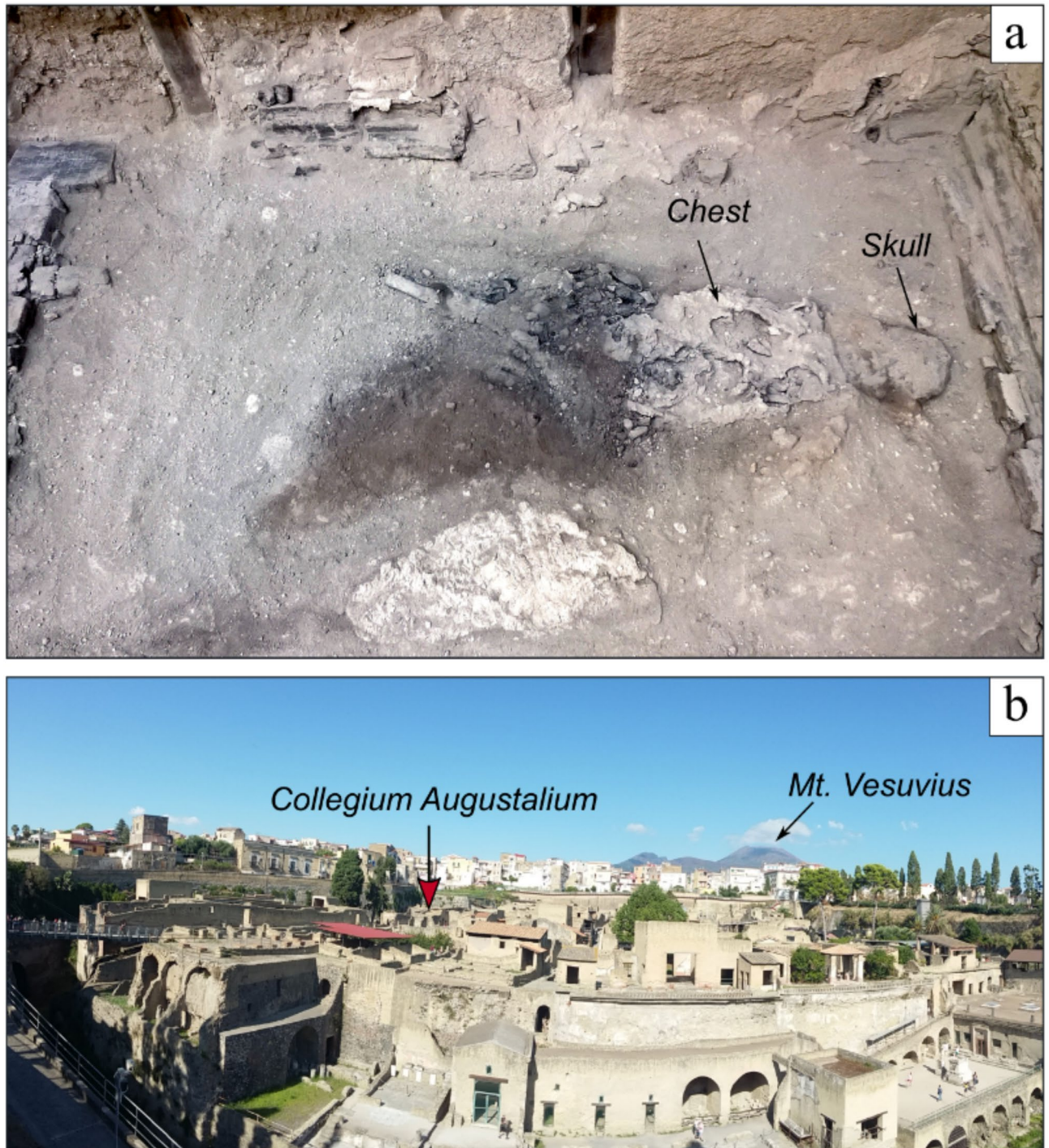


Fig. 1. (a) Carbonized body of the guardian in his wooden bed within the Collegium Augustalium; the vitrified brain remains have been found within his skull. (b) Panoramic eastward view of Herculaneum ruins with Vesuvius volcano in the background, and the location of the Collegium Augustalium within the city.

remnants in the skull are proven to be organic and human brain owing to the preservation of proteins common in human brain tissue and fatty acids typical of both human brain triglycerides and human hair fat⁷, as well as their chemical composition⁸. The glassy nature of this material is suggested because of its black and shiny, obsidian-like appearance⁷ (Fig. 2a). Moreover, exceptionally well-preserved complex networks of neurons, axons, and other neural structures have been revealed by Scanning Electron Microscope (SEM) investigation of the brain remains and those of the spinal cord (Fig. 2) of the guardian⁸, which exclude other types of more common preservation processes, such as saponification^{28,29}. However, an unequivocal origin as an organic glass has not yet been demonstrated, nor the conditions at which such process might have occurred.

The 79 CE Vesuvius eruption killed instantly several thousands of people^{24,27}, but of the approximately 2,000 bodies unearthed throughout the archaeological sites of the Vesuvian area³⁰ the apparently vitrified remains of brain and spinal cord found in the Collegium Augustalium, is the only occurrence of this type⁸. This uniqueness requires very specific and rare conditions for glass formation and preservation. In addition, these unique conditions are completely counterintuitive and so far unexplored, as the temperatures of pyroclastic flow deposits that buried Herculaneum and Pompeii are well documented to have been several hundreds of degrees Celsius^{9,31–33}. Such temperatures are expected to burn and destroy soft tissues, and certainly not lead to quenching. To unravel such a conundrum, here we present analytical and experimental data to constrain the conditions of soft tissue glass formation and preservation in a hot volcanic environment. Our findings have broad implications for material science, volcanology, forensic biology and archaeology.

Materials

The material analysed in this study consists of fragments sampled from within the skull and the spinal cord of a skeleton buried by the pyroclastic flow deposits of the 79 CE Vesuvius eruptions in the archaeological site of Herculaneum (Fig. 1; Table 1).

Material characterisation

The material analysed is made of angular clasts of variable shapes, black to dark grey and shiny under natural or artificial light (Fig. 2a). Clasts were sampled intact, directly from within the skull of the guardian (Fig. 1a). Their dimensions range 0.5–5 mm. Field emission scanning electron microscope (FE-SEM) images (See Methods section) at low magnification show conchoidal surfaces with step-like fractures, with very sharp dihedral angles (Fig. 2b). At higher magnifications, micron-sized spherical voids occur both as isolate, or scattered, or clustered features (Fig. 2c, d). Several features of different shapes, characterised by a very high level of geometrical organization and complexity can be observed on the surfaces of the clasts (Fig. 2e, f), some of which have been recognized and interpreted as integrally preserved human neural structures⁸.

The density of the material averages at 1000 kg m^{-3} . The 3D scanning tomography (see Methods section) shows a very homogeneous material characterised by microporosity of 1.4 vol %. The porosity is made mostly by

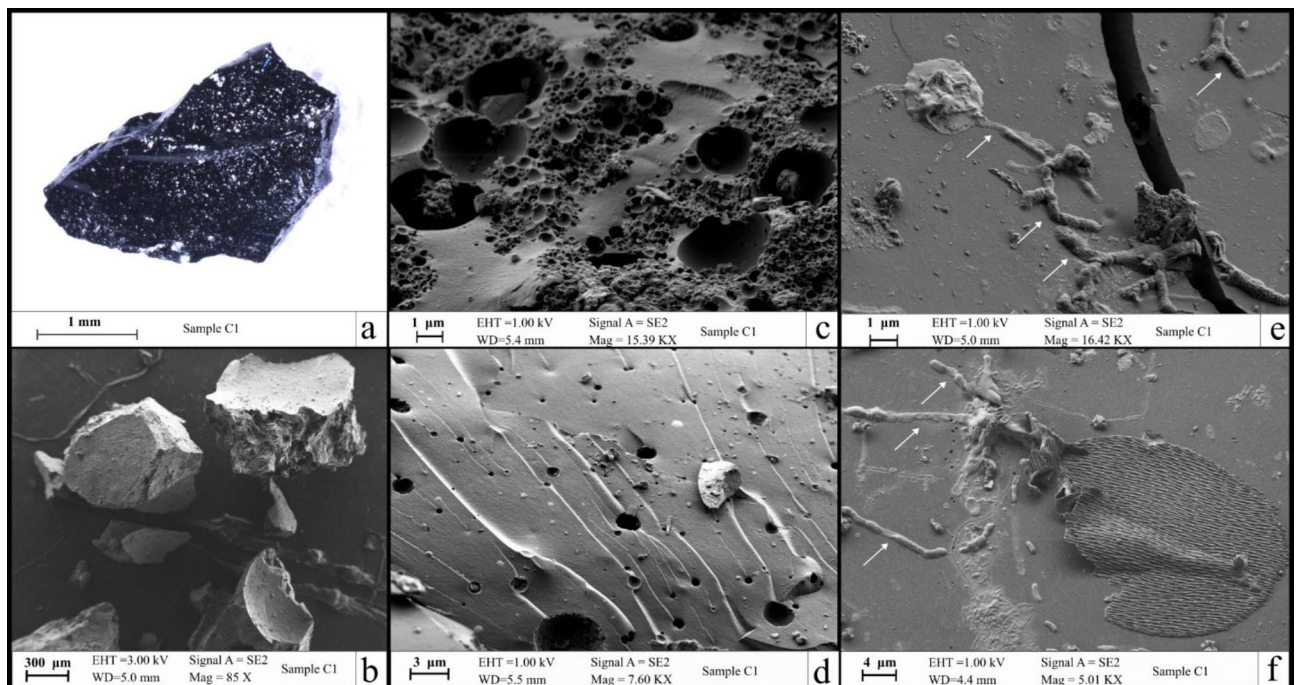


Fig. 2. Images at different magnifications of the C1 sample: (a) optical image under direct light. (b) FE-SEM image showing the angular shape of the fragments. (c), (d) FE-SEM images detail spherical voids clustering and stepped fracture. (e), (f) FE-SEM details of preserved neural structures; white arrows point to the best preserved axons.

ID	Sample	Description	Analytical methods
ERC-2	C1	Several glass fragments from inside the skull	FE-SEM, EDS, Raman, Micro-CT, Calorimetry (C-DSC and F-DSC)
ERC-3	C2a	Glassy bone fragment from the chest	Raman
ERC-4a	C2b	Carbonaceous fragment from the chest	FE-SEM, EDS, Raman
ERC-26	C7	Single glass fragment from inside the skull	FE-SEM, EDS, Raman, Calorimetry (C-DSC), density
ERC-57	C102	Glassy fragment from the chest-5 A	FE-SEM, EDS
ERC-66	C117	Glass fragment from inside the skull	FE-SEM, EDS

Table 1. Summary of samples and analyses conducted for the characterization of the vitrified human brain found at Herculaneum buried by deposits from the 79CE Vesuvius eruption. See Method section for explanation of analytical methods.

micron-sized scattered and isolated spherical voids and subordinate larger and more irregular voids formed by the coalescence of smaller features (Fig. SI1 in Supplementary Information, hereonward SI).

The SEM-EDS (energy dispersive X-ray spectroscopy) analysis (See Methods Section) on groundmass performed during the FE-SEM images acquisition revealed a composition that is predominantly C and O with minor amounts of Na, Cl, K Mg, Al and Si (Fig. SI2).

Differential scanning calorimetry (DSC)

During conventional (C)-DSC analysis (see Methods section), sample C7 was heated at a rate of 25 K min⁻¹ (0.42 K s⁻¹) and exhibited an endothermic event with an onset temperature of 420 °C (Fig. 3). Endothermic events are depicted by upward peaks in Fig. 3. In contrast, a small fragment from sample C1 was analyzed using flash (F)-DSC (see Methods section) at a significantly faster heating rate of 1000 K s⁻¹. This resulted in a similar endothermic event observed at a higher onset temperature of 510 °C (Fig. 3). The C-DSC analysis of sample C7 revealed a subsequent endothermic event peaking around 500 °C, followed by a sharp exothermic event reaching its peak at approximately 530 °C. Interestingly, F-DSC analysis also detected this exothermic event, albeit at a higher peak temperature of 600 °C (Fig. 3).

Assuming the Arrhenius dependence and a balanced thermal history, the two onset temperatures (420 °C for C-DSC and 510 °C for F-DSC) allow a preliminary estimate of the enthalpy change of 390.1 kJ mol⁻¹ associated with relaxation (viscous flow) at the glass transition. Although an Arrhenius dependence is justified over a small range of heating rates, in this case 3.4 log units, the assumption of a matched cooling and heating rate underestimates the fraction of excess enthalpy originating from the thermal history of the samples with mismatched (i.e., this study) cooling and heating rate and its effect on the onset temperature of the glass transition. However, this effect is likely minor. For example, in the technical production of blast furnace slag (silicate) glasses, rapid quenching (~10⁵ K s⁻¹) leads to an excess enthalpy of ~55 kJ mol⁻¹ in relation to standard laboratory heating rates (10 K min⁻¹ = 0.17 K s⁻¹), about 7% of the activation enthalpy of viscous flow at the fictive temperature (740 kJ mol⁻¹)³⁴. Similar small proportions of excess enthalpy are also reported for the production of glass fibers from basaltic rocks for insulation purposes³⁵.

Post-analysis FE-SEM imaging indicated changes in the C-DSC sample during measurement, such as the formation of bubbles and crystals (Fig. 4). Consequently, we associated this alteration in sample texture with degassing, marked by the sharp C-DSC peak slightly above 500 °C. Thus, we assert that the degassing event in C-DSC analysis is preceded by structural relaxation of the material (endothermic event starting at 420 °C) and succeeded by crystallization (at 530 °C). The considerably faster F-DSC analyses suppressed the formation of bubbles and induced crystallization at a higher temperature (600 °C), preceded by structural relaxation (endothermic event starting at 510 °C).

In both C-DSC and F-DSC experiments, samples were subjected to a cooling downscan, returning to room temperature to align with the previous upscan. Subsequent upscans at the same rates did not exhibit any thermal events (Fig. SI3). Consequently, we inferred that after degassing and crystallization the samples were no longer in a glassy state.

Based on C-DSC results obtained from the first upscan up to 620 °C (Fig. 3), we targeted different temperatures by subjecting different fragments of sample C1 to four heating/cooling cycles (run#1–4) to variable maximum temperatures (T_{max}). Specifically, in the first two runs (run#1 and run#2) the sample was heated up to T_{max} of 520 °C. Subsequent cycles were conducted at progressively higher temperatures, with T_{max} of 620 and 670 °C for run#3 and run#4, respectively. C-DSC results are reported in Fig. SI3. By comparing results of the first upscan for samples C7 (Fig. 3) and C1 (Fig. SI3) we notice that the DSC signals are almost overlapping. Minor differences can be due to heterogeneities between samples.

The recovered samples after run#2, run#3 and run#4 were analysed by FE-SEM, EDS and Raman spectroscopy (see Methods section) to detect possible evidence of material transformation and compositional changes.

Post-run#1 and #2 (maximum T of 520 °C) images show that the material did not change its glassy appearance, with surfaces and conchoidal fractures still very sharp, including the preserved neural structures (axons) emerging from the surface of the clast (Fig. SI4.1a–d). However, the clast surface was covered by micron-sized well-formed euhedral cubic crystals, which were not present in the original sample (Fig. 4a, b). EDS analyses showed that the composition of these crystals is pure KCl, whereas the glass maintained its carbonaceous composition (Fig. SI4.1a–d).

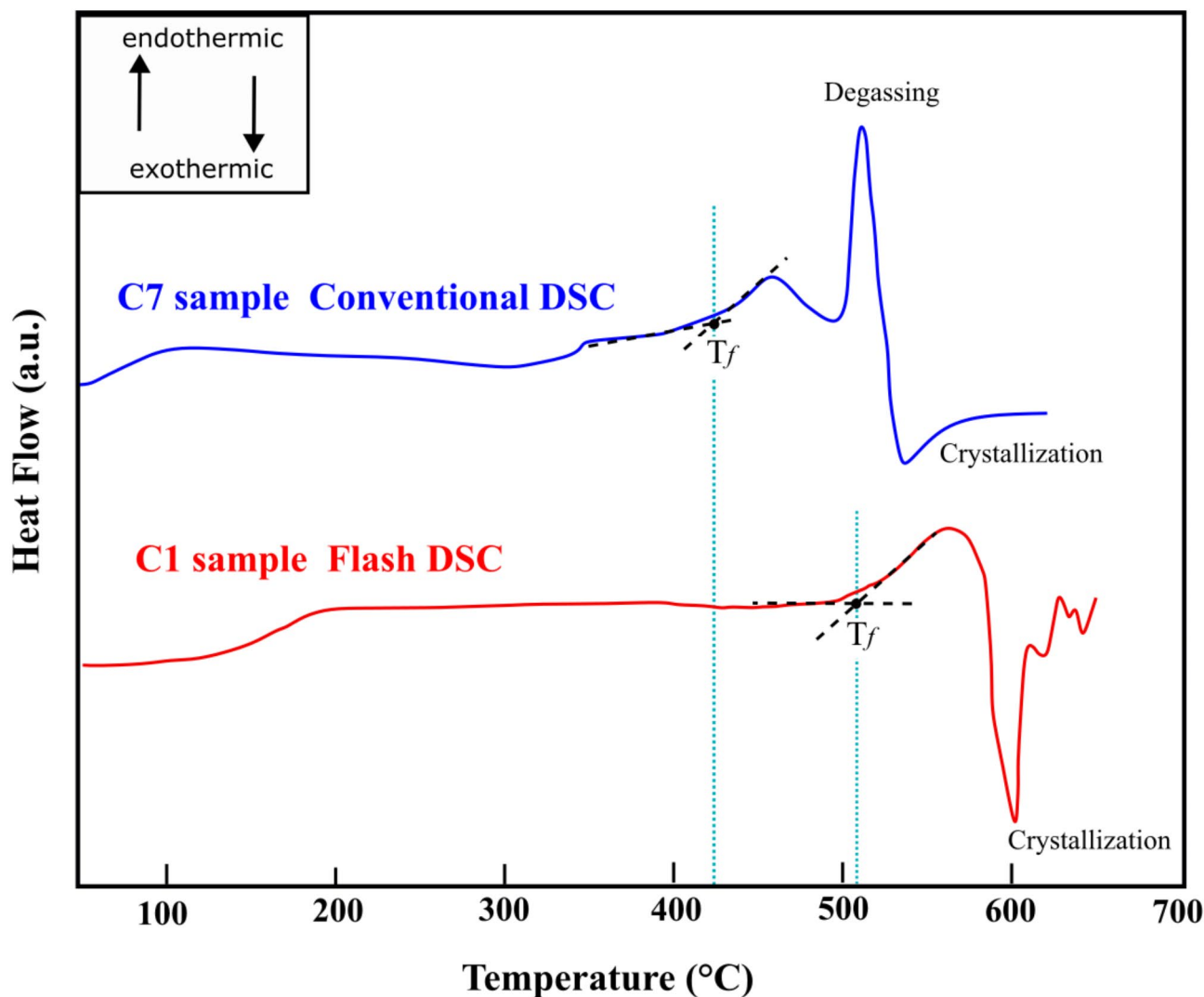


Fig. 3. DSC curves for heating experiments. The blue line represents sample C7 analyzed using C-DSC at a heating rate of 25 K min^{-1} (0.42 K s^{-1}), while the red line represents a fragment of sample C1 analyzed using F-DSC at a heating rate of 1000 K s^{-1} . Upward and downward peaks correspond to endothermic and exothermic events, respectively. The temperature at the onset of relaxation (T_f) is indicated by the intersection of the two tangents drawn to the baseline at the beginning of the first endothermic event. Thermal events are interpreted in the text.

Exposing the material to a higher maximum temperature of $620 \text{ }^\circ\text{C}$ (run#3) resulted in a visible degradation of its initial visual characteristics. Surfaces became more irregular and granular in texture (Fig. 4c). Some evidence of material relaxation was observed in the stepped fractures that appear weakly wavy instead of sharp. KCl crystals are still present but in lesser amounts. The surfaces also show abundant newly formed craters with radial, micron-size, blade-like needle agglomerates emerging from some of them (Fig. 4d).

The EDS composition of the blade-like needles indicates the presence of C, O, Na, P, Ca, K, Mg, Cl and Fe (Fig. SI4.2a-c). The composition of the groundmass instead remained mainly C with only traces of the other components (Fig. SI4.2d-f).

T_{max} in run#4 was $670 \text{ }^\circ\text{C}$. After the experiment, FE-SEM images show a further increase in the process of craterization of the exposed surfaces, transition to granular texture due to crystallization, and the formation of blade-like needle aggregates (Fig. 4e, f). Also, the relaxation of the material appears more evident, with surfaces and edges that become more fluidal in shape.

Raman spectroscopy

Raman analysis (see Methods section) conducted on fragments of the sample C1 groundmass (Fig. 5a) confirmed the organic nature of the material: the spectra are constituted of two main bands centred at $1330\text{--}1370 \text{ cm}^{-1}$ and $1590\text{--}1610 \text{ cm}^{-1}$, called D and G respectively^{36,37}. The G band corresponds to graphite band (carbon)^{36,38}, while the D band indicates the presence of disorder in the graphite structure^{39,40}. D and G display almost equivalent intensity and shape, with the D band slightly wider than the G band.

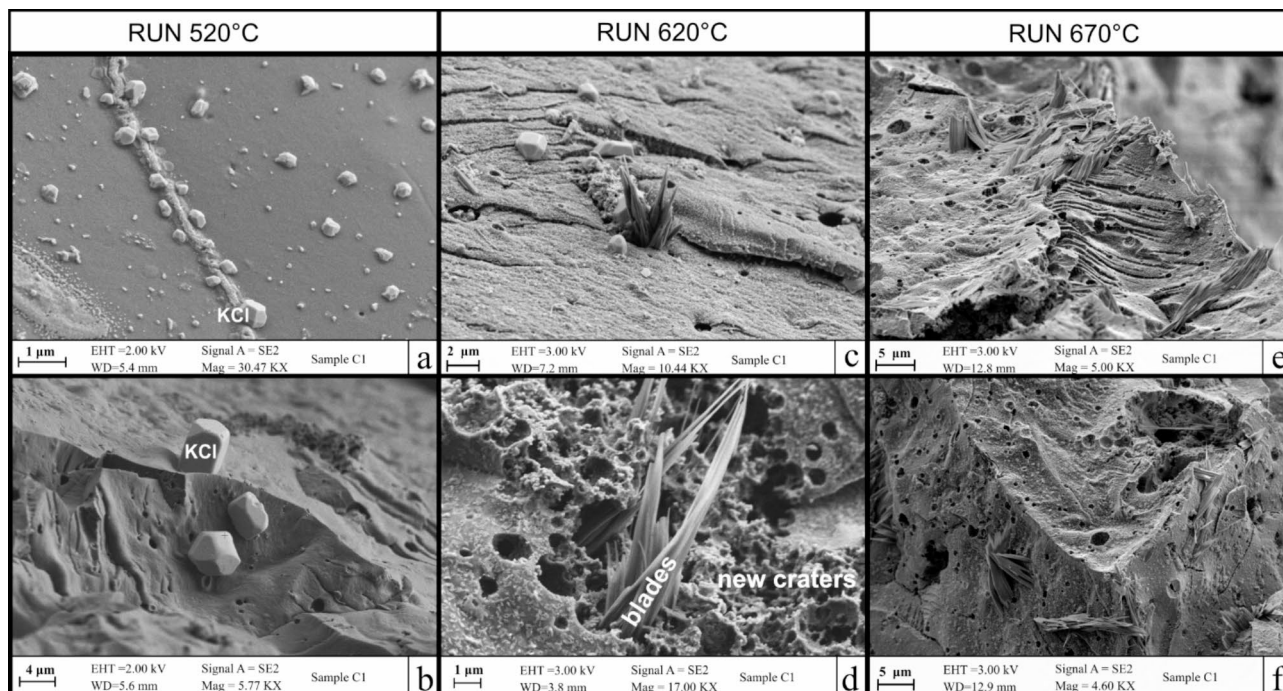


Fig. 4. SEM images (magnification on scale bar) of sample C1 after C-DSC experiments at progressively higher maximum temperatures. **(a)** formation of new small KCl crystals at 520 °C on the undeformed sample surface. **(b)** Detail of the newly formed crystals of KCl at 520 °C on sample surface. **(c)** At 620 °C, crystallization is accompanied by modification of the sample surface which appears more granular and less sharp. **(d)** Detail of sample surface at 620 °C, with formation of craters suggesting degassing and radial blade-like needles emerging from them. **(e), (f)** At 670 °C the surface of the sample becomes more granular with further evidence for relaxation of the material and craterization.

Raman analysis carried out after each experiment at increasing temperature (run#1–4) show changes in shape, intensity and position of the D and G bands with respect to those of the original sample (Fig. 5a). The width of the G band becomes narrower than the D band, a characteristic associated with the transition from amorphous carbonaceous material (pre-run sample) to material with higher structural order after heating. Similar information is given by the increase of D band intensity (I_D) with temperature respect with to G band intensity (I_G) (I_D/I_G in Fig. 5b). The change of I_D is also accompanied by a shift of the D band towards lower wavelengths (Fig. 5b) and a consequent increasing separation from the G band. All the variations are excellent indicators of increasing structural order with thermal maturity, in the low thermal maturity range^{41–43}. These variations are the very first to be shown on this kind of human organic material, and show that at increasing temperature corresponds an increase in structural order in agreement with observation from FE-SEM images (Fig. 4) and with calorimetric evidence for crystallization in the same analysed temperature range (Fig. 3).

Discussion

Although human brain preservation is documented in the archaeological record, it is a relatively infrequent phenomenon. The known mechanisms responsible for such occurrences are dehydration, saponification, tanning, and freezing²⁹, but not vitrification. In addition, neuronal structures are poorly preserved in ancient brains^{44–46}.

Our comprehensive chemical and physical characterization of the material sampled from the skull of a human body buried at Herculaneum by the 79 CE eruption of Mount Vesuvius shows compelling evidence that these are human brain remains, composed of organic glass formed at high temperatures, a process of preservation never previously documented for human or animal tissue, neither brain nor any other kind.

DSC analyses conducted at contrasting heating rates (25 K min^{-1} and 1000 K s^{-1}) revealed consistent patterns indicative of three primary processes occurring within the samples during heating up to 670 °C. The most relevant process is the onset of a structural relaxation of the material, that is the fictive temperature T_f . Figure 3 shows that T_f for the slower heating rate (25 K min^{-1}) is at 420 °C and increases to 510 °C at the faster rate (1000 K s^{-1}). The identified structural relaxation extends for an interval of tens of degrees above T_f and is followed by degassing and crystallization events at higher temperatures (Fig. 3). These processes are accompanied by surface crater formation and KCl crystallization (Fig. 4), likely as a result of degassing of from the glass. The transformation of the material above its fictive temperature T_f is further corroborated by Raman spectroscopy (Fig. 5), which reveals increased order within the carbonaceous component. This transformation inhibits glass formation during experimental cooling, which may explain the absence of thermal events during subsequent upscans.

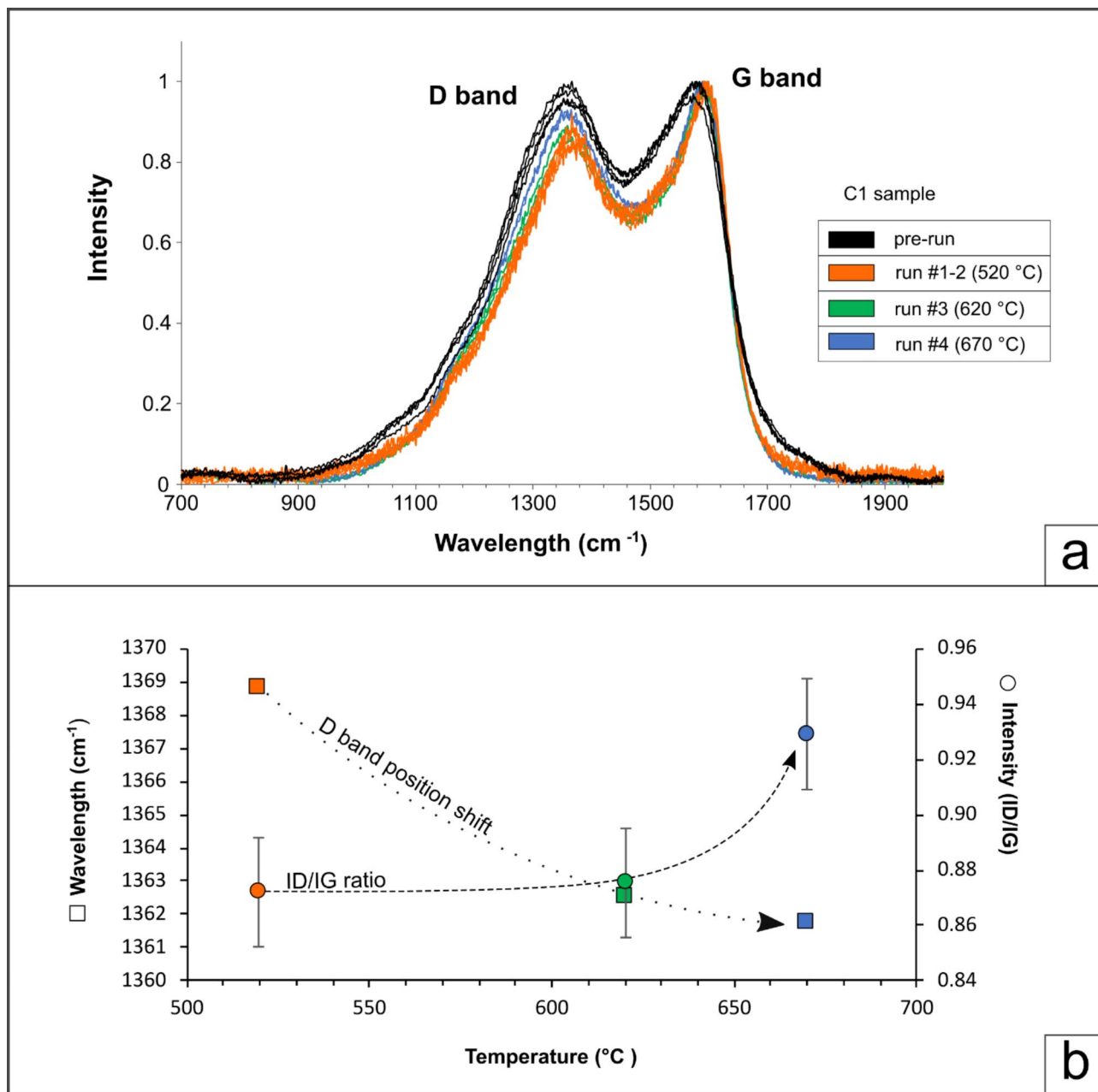


Fig. 5. (a) Representative Raman spectra of sample C1 acquired after each upscan at different T_{\max} ; in black the original, pre-DSC, spectrum in comparison with analyses conducted after experiments, DSC run#1–4. (b) Indicative Raman parameters: ID/IG ratio (circles) and D band position (squares) vs. temperature, colour legend as in a).

To determine the unknown cooling rate experienced by the sample during the volcanic event, and thus the temperature at which the material transformed from human tissue to glass, the temperature dependence of the melt viscosity is required⁴⁷. With this information, cycles of matching heating and cooling at known rates across the glass transition interval are needed to retrieve the unknown cooling rate¹⁷. However, this is not feasible since the temperature dependence of the viscosity for our sample does not exist, preventing the assessment of the natural cooling rate at which the brain was vitrified. Nonetheless, in our experiments the glass underwent structural relaxation at T_f between 420 °C (25 K min⁻¹) and 510 °C (1000 K s⁻¹), allowing us to further investigate the thermal environment where quenching occurred. While this range is a measure of the uncertainties associated with the experiments, we have strong constraints that allow us to identify 510 °C and 1000 K s⁻¹ as the closest approximations for the temperature of liquid to glass transformation and the unknown cooling rate experienced by the sample.

The main constraint is the temperature of the pyroclastic deposits that embed the vitrified brain fragments. The emplacement temperatures of these deposits have been extensively studied by means of palaeomagnetism^{32,33}

and reflectance of charcoal^{9,31}. Both methods provide similar deposition temperatures between 315 °C and 465 °C. The implications of such high deposition temperatures are twofold. First, the preservation of the glass requires the temperature of the embedding pyroclastic material (up to 465 °C) to be (substantially) lower than the brain T_p , because otherwise the glass would have returned to a soft tissue and, at such high temperatures, disintegrated. Second, as a consequence, the vitrification of the brain must have occurred entirely prior to the entombment of the body and the brain inside the pyroclastic material, because glass cannot form during the slow cooling of a pyroclastic deposit.

We therefore infer that within the experimental range of our measured T_f (420–510 °C), the upper bound at 510 °C is the closest to the natural T_p , while 420 °C, which is comparable or lower than the temperature of the embedding deposits, is very unlikely, if not impossible.

This would suggest a very fast process of cooling to vitrify the brain at rates comparable with our experiments at 1000 K s⁻¹. Such fast cooling rates may imply that the brain, while not entirely destroyed during the heating, was likely severely damaged and disaggregated in small sub-centimetric pieces - as they have been found - favouring the heat exchange during cooling. Thus, the only possible scenario for such a process in the context of the 79 CE Vesuvius eruption is that of a short-lived transient passage of a detached very dilute ash cloud surge with internal temperature well above 510 °C^{9,48}. Possibly, the protection by the direct contact with the hot ash cloud given by the thick bones of the skull and spine of the guardian may have helped to prevent complete devolatilization of the brain tissue and the vetrification of the survived parts during rapid cooling. Complete devolatilization affected instead the external soft tissues in both the victims from the city and those discovered in the suburban area, on the beach and in a series of boat-chambers facing the sea⁴⁹.

Therefore, we reconstruct a scenario where a fast, very hot ash cloud was the first deadly event during the 79CE Vesuvius eruption, enveloping victims, including the guardian who was subject to the specific conditions for heating the brain at temperatures well above 510 °C without the (total) destruction of the cerebral tissue. As the ash cloud dissipated (comparison with observed modern ash clouds suggest on order of minutes), the temperature immediately returned to ambient conditions, inducing cooling at rates comparable with our experimental 1000 K s⁻¹ that are very reasonable for cooling upon thermal gradients of several hundred of degrees⁵⁰. The deposit of this early ash cloud surge is present as just few centimeters of ash on ground²² so the bodies were left virtually in open air. The brain then turned into glass during the fast cooling at glass transition temperature close to 510 °C. Later, in agreement with witness accounts and deposit stratigraphy^{9,22,23}, Herculaneum was progressively buried by thick pyroclastic flow deposits, but at lower temperatures^{9,31-33}, so that the unique presence of a vitrified brain could have been preserved until today.

In conclusion, the brain tissue studied here is the only known case of preserved vitrification of human tissue as a result of cooling after heating to very high temperatures. This is the only way by which such a glass type can be preserved in the geological or archaeological record and explains why this is a unique occurrence and preserves the ultra-fine neural structure of the brain⁷.

Methods

The material characterization, included micro-imaging, determination of density, porosity and chemical composition. All necessary permits were obtained for the study of the human specimen from the Ethics Committee for Biomedical Activities, AOU Federico II, Naples, Italy, Protocol N. 101/17. Four un-coated samples (samples C1, C2b, C102 and C117; Table 1) were imaged by a Zeiss Sigma 300 Field emission scanning electron microscope (FE-SEM (Department of Science, University of Roma Tre), at variable operating conditions (e.g., accelerating voltage, as indicated on each image). The densities of samples C1 and C7 were measured by hydrostatic balance (Department of Science, University of Roma Tre). A 3D microtomographic imaging of sample C1 (Table 1) has been acquired by Nikon XT H 225 ST Tomograph, equipped with a Perkin Elmer 1620 (by Remet s.a.s). The chemical composition has been determined by energy dispersive X-ray spectroscopy (EDS). Elemental analyses were performed on a Quantax EDS System, equipped with an XFlash energy-dispersive X-ray detector (Department of Science, University of Roma Tre). EDS operated at acceleration voltages of 15 kV for the measurements. EDS analysis was acquired using a 16 μs dwell time per pixel. The EDS spectra were analysed with ESPRIT 2 software. Raman spectroscopy was performed using a Jobin Yvon micro-Raman LabRam system (Department of Science, University of Roma Tre). A neodymium-yttrium-aluminum-garnet (Nd:YAG) laser at 532 nm (green laser) was used in a backscattering geometry using a 600 grooves mm⁻¹ spectrometer grating and Charge Coupled Device (CCD) photon detector. Spectra were collected at 700–2300 cm⁻¹ (first order Raman spectrum) on a 5 μm diameter spot, with a 50X optical objective.

The samples were subjected to differential scanning calorimetry analysis (DSC) which involved the investigation of endothermic and exothermic events during the heating and cooling processes of samples C1 and C7. Two types of calorimetry techniques, conventional (C)-DSC and flash (F)-DSC, were employed for this study. Initially, two samples underwent high-temperature treatments at relatively slow rates of heating and cooling using the C-DSC apparatus (Netzsch Pegasus, Department of Science, University of Roma Tre). C-DSC measurements were conducted under N2 5.0 atmosphere (flow rate 30 ml min⁻¹). The temperature calibration was performed up to ~1050°C using the melting points of reference materials (In, Sn, Bi, Zn, Al, Ag, and Au). Baseline measurements were conducted with two empty Pt crucibles. C-DSC samples experienced heating and cooling rates of 25 K min⁻¹. Specifically, the C7 sample (20 mg) underwent a single heating/cooling cycle with a maximum temperature (T_{max}) of 620°C. One fragment of the sample C1 (20 mg) underwent four heating/cooling cycles with T_{max} values first at 520°C, then repeated at 520°C, and then increased to 620°C and 670°C. Post-treatment, the samples were analysed using FE-SEM, EDS, and Raman techniques, utilizing the same instruments and settings as previously described. Additionally, the F-DSC (Clausthal University of Technology) was employed to explore much faster heating and cooling rates for fragments from the same sample C1 studied by C-DSC. We used the UFH1 sensor (operating up to 1,000°C and cooling/heating rated of 30,000 K s⁻¹).

Before measuring, the sensor underwent a two-step thermal treatment following the manufacturer's protocols: (1) a conditioning program to remove thermal history, and (2) a thermocouple correction program. F-DSC temperature calibration was performed using the melting temperature of aluminum ($T_m = 660.4^\circ\text{C}$) and indium ($T_m = 156.6^\circ\text{C}$). Two cycles of heating and two cycles of cooling were conducted on sample C1. The procedure involved an initial heating cycle at 1000 K s^{-1} , followed by a downscan at the same rate of 1000 K s^{-1} .

Data availability

All data from this study are available within the article. Additional data that support the findings of this study are available from the corresponding authors on reasonable request.

Received: 12 October 2024; Accepted: 31 January 2025

Published online: 27 February 2025

References

- Zanotto, E. D. & Mauro, J. C. The glassy state of matter: its definition and ultimate fate. *J. Non-Cryst. Solids*. **471**, 490–495 (2017).
- Tool, A. Q. Relation between inelastic deformability and thermal expansion of glass in its annealing range. *J. Am. Ceram. Soc.* **29** (9), 240–253 (1946).
- Chen, Z. et al. Calorimetric determination of fragility in glass forming liquids: T f vs. T g-onset methods. *Eur. Phys. J. E.* **37**, 1–7 (2014).
- Zheng, Q. et al. Understanding glass through differential scanning calorimetry. *Chem. Rev.* **119** (13), 7848–7939 (2019).
- Wovk, B. Thermodynamic aspects of vitrification. *Cryobiology* **60** (1), 11–22 (2010).
- Hunt, C. J. Cryopreservation of human stem cells for clinical application: A review. *Transfus. Med. Hemotherapy*. **38** (2), 107–123 (2011).
- Petrone, P. et al. Preservation of neurons in an AD 79 vitrified human brain. *PLoS ONE*. **15** (10), e0240017 (2020a).
- Petrone, P. et al. Heat-induced brain vitrification from the Vesuvius eruption in CE 79. *N. Engl. J. Med.* **382** (4), 383–384 (2020b).
- Pensa, A., Giordano, G., Corrado, S. & Petrone, P. P. A new hazard scenario at Vesuvius: Deadly thermal impact of detached ash cloud surges in 79CE at Herculaneum. *Sci. Rep.* **13** (1), 5622 (2023).
- Moynihan, C. T., Easteal, A. J., De Bolt, M. A. & Tucker, J. Dependence of the fictive temperature of glass on cooling rate. *J. Am. Ceram. Soc.* **59** (1–2), 12–16 (1976).
- Webb, S. L., Knoche, R. & Dingwell, D. B. Determination of silicate liquid thermal expansivity using dilatometry and calorimetry. *Eur. J. Mineral.* **1**, 95–104 (1992).
- Knoche, R., Dingwell, D. B., Seifert, F. A. & Webb, S. L. Non-linear properties of supercooled liquids in the system $\text{Na}_2\text{O-SiO}_2$. *Chem. Geol.* **116** (1–2), 1–16 (1994).
- Potuzak, M., Nichols, A. R., Dingwell, D. B. & Clague, D. A. Hyperquenched volcanic glass from Loihi Seamount, Hawaii. *Earth Planet. Sci. Lett.* **270** (1–2), 54–62 (2008).
- Guo, X. et al. Unified approach for determining the enthalpic fictive temperature of glasses with arbitrary thermal history. *J. Non-Cryst. Solids*. **357** (16–17), 3230–3236 (2011).
- Gottsmann, J. & Dingwell, D. B. The thermal history of a spatter-fed lava flow: The 8-ka pantellerite flow of Mayor Island, New Zealand. *Bull. Volcanol.* **64**, 410–422 (2002).
- Scarani, A. et al. Timescale of emplacement and rheomorphism of the Green Tuff Ignimbrite (Pantelleria, Italy). *J. Geophys. Res. Solid Earth*, **128**(7), (2023). e2022JB026257.
- Scarani, A. et al. Determination of cooling rates of glasses over four orders of magnitude. *Contrib. Miner. Petrol.* **177** (3), 35 (2022).
- Hughes, A. et al. Shear localisation, strain partitioning and frictional melting in a debris avalanche generated by volcanic flank collapse. *J. Struct. Geol.* **140**, 104132 (2020).
- Çalışkanoglu, A. Z., Camara, A. S., Cimarelli, C., Dingwell, D. B. & Hess, K. U. Experimental generation of fulgurite under realistic lightning discharge conditions. *Sci. Rep.* **13** (1), 11685 (2023).
- Han, Z. et al. Vitrification and nanowarming enable long-term organ cryopreservation and life-sustaining kidney transplantation in a rat model. *Nat. Commun.* **14**, 3407. <https://doi.org/10.1038/s41467-023-38824-8> (2023).
- Pegg, D. E. The role of vitrification techniques of cryopreservation in reproductive medicine. *Hum. Fertil. (Camb)*. **8** (4), 231–239 (2005).
- Sigurdsson, H., Carey, S., Cornell, W. & Pescatore, T. The eruption of Vesuvius in AD 79. *Natl. Geogr. Res.* **1**, 3 (1985). <https://digit.alcommons.uri.edu/gsofacpubs/1114>
- Sigurdsson, H., Cashdollar, S. & Sparks, R. S. J. The eruption of Vesuvius in A.D. 79: Reconstruction from historical and volcanological evidence. *Am. J. Archeol.* **86**, 39–51 (1982).
- Giacomelli, L., Perrotta, A., Scandone, R. & Scarpati, C. The eruption of Vesuvius of 79 AD and its impact on human environment in Pompeii. *Episodes J. Int. Geosci.* **26** (3), 235–238 (2003).
- Gurioli, L., Houghton, B. F., Cashman, K. V. & Cioni, R. Complex changes in eruption dynamics during the 79 AD eruption of Vesuvius. *Bull. Volcanol.* **67**, 144–159 (2005).
- Doronzo, D. M. et al. The 79 CE eruption of Vesuvius: A lesson from the past and the need of a multidisciplinary approach for developments in volcanology. *Earth Sci. Rev.* **231**, 104072 (2022).
- Petrone, P. The Herculaneum victims of the 79 AD Vesuvius eruption: A review. *J. Anthropol. Sci.* **97**, 1–22 (2019).
- Ubelaker, D. H. & Zarenko, K. M. Adipocere: what is known after over two centuries of research. *Forensic Sci. Int.* **208** (1–3), 167–172 (2011).
- Morton-Hayward, A. L., Anderson, R. P., Saupe, E. E., Larson, G. & Cosmidis, J. G. Human brains preserve in diverse environments for at least 12 000 years. *Proc. R. Soc. B*, **291** 20232606 (2024). (2019).
- De Carolis, E., Patricelli, G. & Raimondi Cominesi, A. Rinvenimenti Di Corpi Umani Nel Suburbio Pompeiano E Nei Siti Di Ercolano E Stabia. *Riv Studi Pompeiani*. **24**, 11–32 (2013).
- Caricchi, C., Vona, A., Corrado, S., Giordano, G. & Romano, C. 79 AD Vesuvius PDC deposits' temperatures inferred from optical analysis on woods charred in-situ in the Villa dei Papiri at Herculaneum (Italy). *J. Volcanol. Geoth. Res.* **289**, 14–25 (2014).
- Cioni, R., Gurioli, L., Lanza, R. & Zanello, E. Temperatures of the AD 79 pyroclastic density current deposits (Vesuvius, Italy). *J. Geophys. Res. Solid Earth*, **109**(B2) (2004).
- Giordano, G. et al. Thermal interactions of the AD79 Vesuvius pyroclastic density currents and their deposits at Villa Dei Papiri (Herculaneum archaeological site, Italy). *Earth Planet. Sci. Lett.* **490**, 180–192 (2018).
- Pronina, N., Krüger, S., Bornhöft, H., Deubener, J. & Ehrenberg, A. Cooling history of a wet-granulated blast furnace slag (GBS). *J. Non-Cryst. Solids*. **499**, 344–349 (2018).
- Yue, Y., von der Ohe, R. & Jensen, S. L. Fictive temperature, cooling rate, and viscosity of glasses. *J. Chem. Phys.* **120**, 8053–8059 (2004).
- Tuinstra, F. & Koenig, J. L. Raman spectrum of graphite. *J. Chem. Phys.* **53**, 1126–1130 (1970).

37. Friedel, R. & Carlson, G. Difficult carbonaceous materials and their infra-red and Raman Spectra. Reassignments for coal spectra. *Fuel* **51**, 194–198 (1972).
38. Pimenta, M. A. et al. Studying disorder in graphite-based systems by Raman spectroscopy. *Phys. Chem. Chem. Phys.* **9**, 1276–1290 (2007).
39. Negri, F. et al. Resonance Raman contribution to the D band of carbon materials: Modeling defects with quantum chemistry. *J. Chem. Phys.* **120**, 11889–11900 (2004).
40. Lünsdorf, N. K. Raman spectroscopy of dispersed vitrinite – methodical aspects and correlation with reflectance. *Int. J. Coal Geol.* **153**, 75–86 (2016).
41. Henry, D. G., Jarvis, I., Gillmore, G. & Stephenson, M. Raman spectroscopy as a tool to determine the thermal maturity of organic matter: Application to sedimentary, metamorphic and structural geology. *Earth Sci. Rev.* **198**, 102936 (2019).
42. Schito, A., Romano, C., Corrado, S., Grigo, D. & Poe, B. Diagenetic thermal evolution of organic matter by Raman spectroscopy. *Org. Geochem.* **106**, 57–67. <https://doi.org/10.1016/j.orggeochem.2016.12.006> (2017).
43. Schito, A. et al. Calibrating carbonization temperatures of wood fragments embedded within pyroclastic density currents through Raman Spectroscopy. *Minerals* **12** (2), 203. <https://doi.org/10.3390/min12020203> (2022).
44. Doran, G. H. et al. Anatomical, cellular and molecular analysis of 8,000-yr-old human brain tissue from the Windover archaeological site. *Nature* **323** (6091), 803–806 (1986).
45. Kim, M. J. et al. Human mummified brain from a medieval tomb with lime-soil mixture barrier of the Joseon Dynasty, Korea. *Int. J. Osteoarchaeol.* **18** (6), 614–623 (2008).
46. Tkocz, I., Bytzer, P. & Bierring, F. Preserved brains in medieval skulls. *Am. J. Phys. Anthropol.* **51**, 197–202 (1979).
47. Stabile, P. et al. The effect of iron and alkali on the nanocrystal-free viscosity of volcanic melts: A combined Raman spectroscopy and DSC study. *Chem. Geol.* **559**, 119991. <https://doi.org/10.1016/j.chemgeo.2020.119991> (2021).
48. Mastrolorenzo, G., Petrone, P., Pappalardo, L. & Guarino, F. M. Lethal thermal impact at periphery of pyroclastic surges: Evidences at Pompeii. *PLoS ONE*, **5**(6), e11127 (2010).
49. Petrone, P. et al. A hypothesis of sudden body fluid vaporization in the 79 AD victims of Vesuvius. *PLoS ONE*. **13** (9), e0203210 (2018).
50. Thomas, R. M. E. & Sparks, R. S. J. Cooling of tephra during fallout from eruption columns. *Bull. Volcanol.* **54**, 542–553 (1992).

Acknowledgements

The authors would like to thank Dr. Francesco Sirano, director of the Herculaneum Archaeological Park, for allowing the study of the human biological samples used in this manuscript (Permit number “Parco Archeologico di Ercolano MIBAC-PA-ERCO, MBAC-PA-ERCO 0003371 13/09/2018, CI. 16.19. 40/1”). All necessary permits were obtained for the study of the human specimen from the Ethics Committee for Biomedical Activities, AOU Federico II, Naples, Italy, Protocol N. 101/17. G.G. acknowledges the grant to the Department of Science, Roma Tre University (MIUR-Italy Dipartimenti di Eccellenza, Art. 1, Comm. 314–337, L. 232/2016). D. Di Genova acknowledges the funding from the European Research Council (ERC) under the European Union’s Horizon Europe research and innovation programme (NANOVOLC, ERC Consolidator Grant – No. 101044772). D. Di Genova acknowledges the Deutsche Forschungsgemeinschaft (DFG) project DI 2751/2–1. D. Di Genova acknowledges funding from the European Union’s – Next Generation EU, Missione 4 Componente 1 CUP B53D23007230006. The authors also acknowledge an anonymous reviewer and C. D’Orlando for their constructive comments.

Author contributions

G.G. and P.P.P. conceived and designed the study; A.P., A.V., A.F., G.G. performed analyses for material characterization; A.P., A.V., G.G. performed C-DSC analyses; D.D.G., R.A.-M., J.D. performed F-DSC analyses; A.P., C.R., A.V., A.F. performed Raman analyses. All authors discussed the results and contributed to the writing and commented on the manuscript.

Declarations

Competing interests

The authors declare no competing interests.

Additional information

Supplementary Information The online version contains supplementary material available at <https://doi.org/10.1038/s41598-025-88894-5>.

Correspondence and requests for materials should be addressed to G.G.

Reprints and permissions information is available at www.nature.com/reprints.

Publisher’s note Springer Nature remains neutral with regard to jurisdictional claims in published maps and institutional affiliations.

Open Access This article is licensed under a Creative Commons Attribution-NonCommercial-NoDerivatives 4.0 International License, which permits any non-commercial use, sharing, distribution and reproduction in any medium or format, as long as you give appropriate credit to the original author(s) and the source, provide a link to the Creative Commons licence, and indicate if you modified the licensed material. You do not have permission under this licence to share adapted material derived from this article or parts of it. The images or other third party material in this article are included in the article's Creative Commons licence, unless indicated otherwise in a credit line to the material. If material is not included in the article's Creative Commons licence and your intended use is not permitted by statutory regulation or exceeds the permitted use, you will need to obtain permission directly from the copyright holder. To view a copy of this licence, visit <http://creativecommons.org/licenses/by-nc-nd/4.0/>.

© The Author(s) 2025